Electrically small water-based hemispherical dielectric resonator antenna

Jacobsen, Rasmus E.; Lavrinenko, Andrei V.; Arslanagić, Samel

Published in:
Applied Sciences (switzerland)

Link to article, DOI:
10.3390/app9224848

Publication date:
2019

Document Version
Publisher's PDF, also known as Version of record

applied sciences

MDPI

Article

Electrically Small Water-Based Hemispherical Dielectric Resonator Antenna

Rasmus E. Jacobsen [1,*], Andrei V. Lavrinenko [1] and Samel Arslanagić [2]

[1] Department of Photonics Engineering, Technical University of Denmark, 2800 Kgs. Lyngby, Denmark; alav@fotonik.dtu.dk

[2] Department of Electrical Engineering, Technical University of Denmark, 2800 Kgs. Lyngby, Denmark; sar@elektro.dtu.dk

* Correspondence: rajac@fotonik.dtu.dk

Received: 10 October 2019; Accepted: 5 November 2019; Published: 13 November 2019

Abstract: Recently, water has been proposed as an interesting candidate for use in applications such as tunable microwave metamaterials and dielectric resonator antennas due to its high and temperature-dependent permittivity. In the present work, we considered an electrically small water-based dielectric resonator antenna made of a short monopole encapsulated by a hemispherical water cavity. The fundamental dipole resonances supported by the water cavity were used to match the short monopole to its feed line as well as the surrounding free space. Specifically, a magnetic (electric) dipole resonance was exploited for antenna designs with a total efficiency of 29.5% (15.6%) and a reflection coefficient of −24.1 dB (−10.9 dB) at 300 MHz. The dipole resonances were effectively excited with different monopole lengths and positions as well as different cavity sizes or different frequencies in the same cavity. The overall size of the optimum design was 18 times smaller than the free-space wavelength, representing the smallest water-based antenna to date. A prototype antenna was characterized, with an excellent agreement achieved between the numerical and experimental results. The proposed water-based antennas may serve as cheap and easy-to-fabricate tunable alternatives for use in very high frequency (VHF) and the low end of ultrahigh frequency (UHF) bands for a great variety of applications.

Keywords: dielectric resonator antenna; electrically small antenna; Mie resonances; tunable antennas; water-based

1. Introduction

Modern technology calls for increasingly smaller designs, which in turn ultimately requires increasingly smaller antennas. Even though electrically small antennas have been studied for decades [1–9], their inherently poor matching, low radiation efficiency, and narrow bandwidth pose a serious design obstacle. The matching issue is traditionally tackled with appropriate matching networks; however, such solutions suffer from narrow bandwidths, high tolerance requirements, and modest efficiencies [2]. While some recent approaches toward efficient small antennas have involved either specific shaping of the radiator or addition of conductors around it [3–6], as well as exploiting artificial metamaterials (MMs) and MM-inspired structures [7–9], a more traditional approach to reduce the antenna size has been to load it with a high-permittivity material. Such antennas, known as dielectric resonator antennas (DRAs), rely on resonances supported in high-permittivity structures. A great variety of DRAs has been proposed and demonstrated [10], and, very often, expensive high-permittivity ceramics are used as the dielectric material. To this end, it is interesting to pay attention to water as an alternative material [11]. With its relatively high frequency and temperature-dependent permittivity in the microwave frequency range [12], water holds a great potential as an inexpensive, abundant, and

biofriendly material for not only tunable antennas [11,13–22] but also more broadly as inclusions in MMs and metasurfaces (MSs) [22–27] with tunable dynamic properties. These tunable properties can potentially be used for sensing as well.

Indeed, several water-based DRAs have already been demonstrated [11,13–18], with effective excitation of resonances in water cavities. Cylindrical [13], rectangular [14], and bottle-shaped [18] cavities have been investigated. These antennas mainly operate in the very high frequency (VHF) and the low end of ultrahigh frequency (UHF) bands due to water losses at higher frequencies. Another type of water-based antenna that exploits conductive liquids (e.g., salt water) [19–22] has also been reported. The operational frequency of these antennas can be tuned through a simple change of the conductive liquid volume. The electrical size of an antenna is defined as k_0a, with a being the radius of the so-called Wheeler's radian sphere (the smallest possible sphere enclosing the antenna), $k_0 = 2\pi/\lambda_0$ being the free-space wavenumber, and λ_0 being the free-space wavelength. In the presence of a ground plane, $k_0a \leq 0.5$ in order for the antenna to be qualified as electrically small [5]. Following this definition, we find that most of the water-based antennas demonstrated thus far are not electrically small.

The purpose of the present work was to investigate an electrically small water-based DRA consisting of a short monopole antenna encapsulated by a hemispherical water cavity and fed against a large ground conducting plane. The working principle of the proposed DRA relies on the fundamental electric and magnetic dipole resonances (equivalent to the transverse magnetic (TM) and transverse electric (TE) modes, respectively), which can be excited in the high-permittivity water cavity. The spherical shape of the cavity maximizes the antenna volume, making it possible to obtain much smaller water-based antennas compared to any of those reported thus far. Specifically, the size of the smallest antenna proposed presently is $\lambda_0/18$, representing the smallest water-based antenna to date. On the other hand, the dipole resonances in the water cavity are used to effectively match an otherwise inefficient short monopole antenna to its feed line as well as the surrounding free space. The length and the position (with respect to the water cavity) of the short monopole were determined for the optimal performance of the DRAs. A prototype antenna operating at 300 MHz was characterized, and measurements exhibited an excellent agreement with the numerical predictions.

The rest of the paper is organized as follows. Section 2 introduces the configuration of the water-based DRA as well as the numerical model. Section 3 presents the numerical and experimental results. Section 4 includes a summary and the conclusions of this work. Appendices A and B contain the antenna parameter definitions and additional results, respectively. Throughout the work, the time factor $\exp(j\omega t)$, where ω is the angular frequency and t is the time, was assumed and suppressed.

2. Configuration

The water-based DRA is shown in Figure 1. The hemispherical cavity has radius r_w, and the feed line is a coaxial transmission line with an inner and outer radii of $r_i = 0.92$ mm and $r_o = 2.99$ mm, respectively, and a dielectric material with the relative permittivity of $\varepsilon_c \approx 2.1$. The characteristic impedance of the feed line is 48.75 Ω, and its length was set to $l_c = 10$ mm in the numerical model. The monopole of length l_m is displaced from the center by distance x_m. A Cartesian coordinate system was introduced, as shown in Figure 1. The permittivity of water was described by the Debye model [12]. A model of the water-based DRA was built in COMSOL Multiphysics 5.3 [28], which was used in all numerical calculations. The model consisted of the DRA enclosed by a hemisphere of free space and with a perfect electric conductor (PEC) plane as the ground. An outer perfectly matched layer (PML) terminated the free-space hemisphere. A matched port was placed on the bottom of the transmission line, as shown in Figure 1. The input power was set to 1 W.

See Appendix A for definitions and more details of the antenna parameters used in this work.

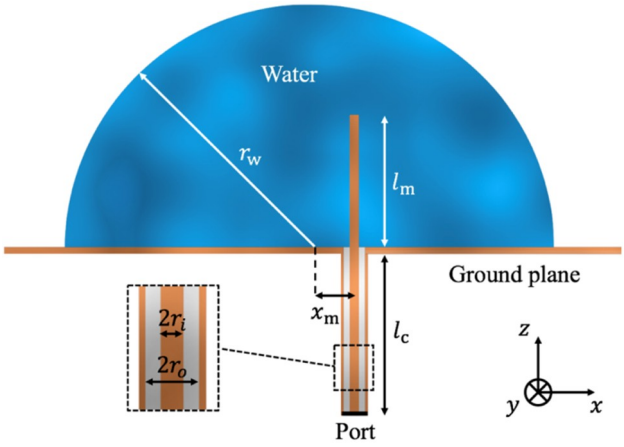

Figure 1. A sketch of the water-based dielectric resonator antenna (DRA).

3. Results and Discussion

We designed the antenna to operate at 300 MHz and 20 °C, where the relative permittivity of water was 80.2 – *j*1.34. However, to study the influence of the dispersion of water, we compared it with an antenna designed for 1000 MHz, where the relative permittivity of water was 79.9 – *j*4.46, clearly showing higher losses. We used two designs exciting different resonances in the hemisphere. With the PEC plane imaging the induced volume currents inside the hemisphere, the resonances will effectively be similar to the ones in the full sphere (the resonant properties of spherical configurations are known [29] also when water is used as the dielectric [30] and were utilized presently for the design of water-based DRAs. See also Appendix B.1 for more details). After a systematic parametric study of the two parameters l_m and x_m, the most efficient designs were found, and the final results are summarized in Table 1 for both frequencies. The total efficiency (η_{eff}) is shown as a function of frequency in Figure 2a for both designs. At 300 MHz, a magnetic (electric) dipole resonance could be excited in a sphere with the radius 55.18 mm (78.53 mm) equal to $\lambda_0/18$ ($\lambda_0/14$). The maximum total efficiency for the magnetic (electric) dipole antenna was 29.5% (15.6%). For comparison, the total efficiency without water was only 0.037% (0.0013%), with almost total reflection of the input power. Thus, introducing water not only matched the antenna to the transmission line but also to the ambient free space, as also confirmed by the reflection coefficient (S_{11}) and radiation efficiency (η_{rad}) in Figure 2b. The magnetic dipole resonance in a water sphere is the most pronounced [30]. This was also the case here, as illustrated in Figure 2. However, due to the losses in water, both antennas absorbed (i.e., dissipated) more power than they radiated: the magnetic (electric) dipole antenna absorbed 70.1% (76.3%). Compared to the antennas at 1000 MHz, where the losses of water were even greater, we found that the total efficiency dropped by approximately a factor of 3 (see Table 1).

As both resonances could be excited in a single hemisphere but at different frequencies, we fabricated one antenna, where the position and the length of the monopole could be adjusted for each resonance type. The antenna was fabricated by hollowing out a hemisphere with the radius 55.18 mm in a Rohacell 51 HF block. The permittivity of Rohacell 51 HF was measured to be 1.075 [26]. The Rohacell block was then glued to an aluminum plate in which holes were drilled for insertion of the monopole antennas and water. Photographs of the antenna are shown in Figure 3a. Two holes ($x_m = 7$ mm and $x_m = 0$ mm) and two monopole antennas ($l_m = 43.6$ mm and $l_m = 15.3$ mm) were made so that both dipole DRA resonances could be excited. The ground plane was realized by attaching a circular aluminum plate with a diameter of 1 m to the antenna. The antenna was mounted on a tripod with a rotating joint, and the reflection coefficient was measured with an Anritsu MS2024B vector network analyzer calibrated for 50 Ohm matching.

Table 1. Geometrical and important antenna parameters for magnetic and electric dipole antennas designed for 300 and 1000 MHz.

Parameter	300 MHz		1000 MHz	
	Magnetic Dipole	**Electric Dipole**	**Magnetic Dipole**	**Electric Dipole**
r_w (mm)	55.18	78.53	16.56	22.5
l_m (mm)	43.6	16	15.4	7.9
x_m (mm)	7	0	2.4	0
f (MHz)	300	298	1000	1010
G_{real} (dBi)	0.16	–3.1	–4.3	–8.2
η_{eff}	29.5%	15.6%	9.1%	4.8%
η_{rad}	29.6%	17%	9.5%	4.8%
$\|S_{11}\|$ (dB)	–24.1	–10.9	–13.7	–19.1
Z_A (Ω)	$43 - j0.7$	$28 - j6.7$	$32.1 - j0.9$	$40 + j3.5$
k_0a (rad)	0.35	0.46	0.35	0.48
FBW_{3dB}	7.81%	2.85%	24%	11.4%
Q_{ratio}	1.06	22.4	1.10	21.5

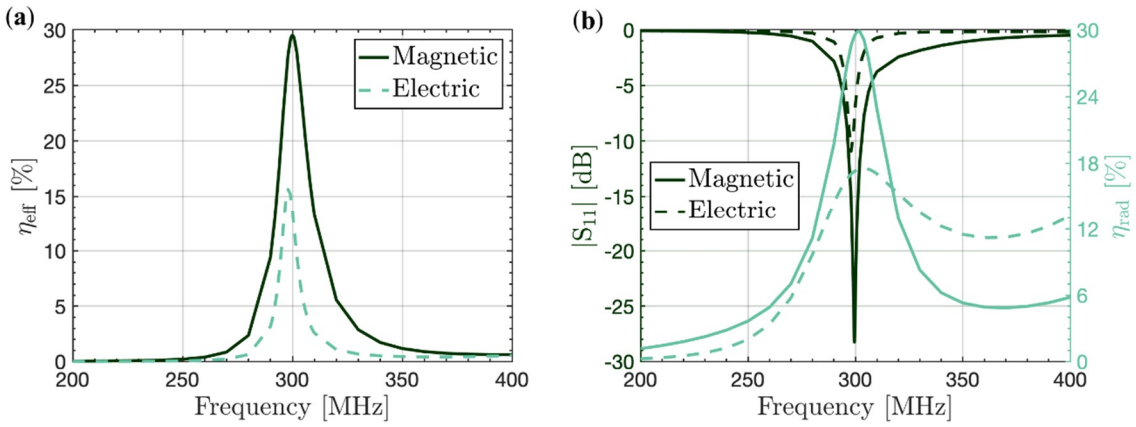

Figure 2. The numerical results for (**a**) total efficiency and (**b**) reflection coefficient and radiation efficiency as functions of frequency. Water temperature was 20 °C.

The water inlet made it easy to insert and extract water from the antenna. With no water, we measured a reflection coefficient of 0 dB with both monopole antennas. The measured reflection coefficients for the antenna filled with water are shown in Figure 3b. Clearly, the reflected power was reduced at the resonance frequencies for specific combinations of x_m and l_m. When the monopole antenna was positioned in the center of the hemisphere, the magnetic dipole resonance was not excited, and thus most of the power was reflected at 300 MHz. The electric dipole was optimally excited around 420 MHz with $x_m = 0$ and $l_m = 43.6$ mm. The numerical results are included in Figure 3b, showing full agreement with the measurements. The small mismatch of 0.4 MHz in frequency between experimental and numerical reflection minimum can be explained by a small difference in temperature and/or water filling in the hemisphere.

The water was removed from the hemisphere and then filled in to check the reproducibility of the measurements. This was done five times, and only a slight difference was observed between the measurements, with the values of the mean and maximum deviation being 299.725 MHz and 0.375 MHz, respectively. We found some differences in the magnitude of the reflection coefficient too (between –23 and –35 dB), but because its absolute value was very low, these differences could have come from small changes in the experimental conditions.

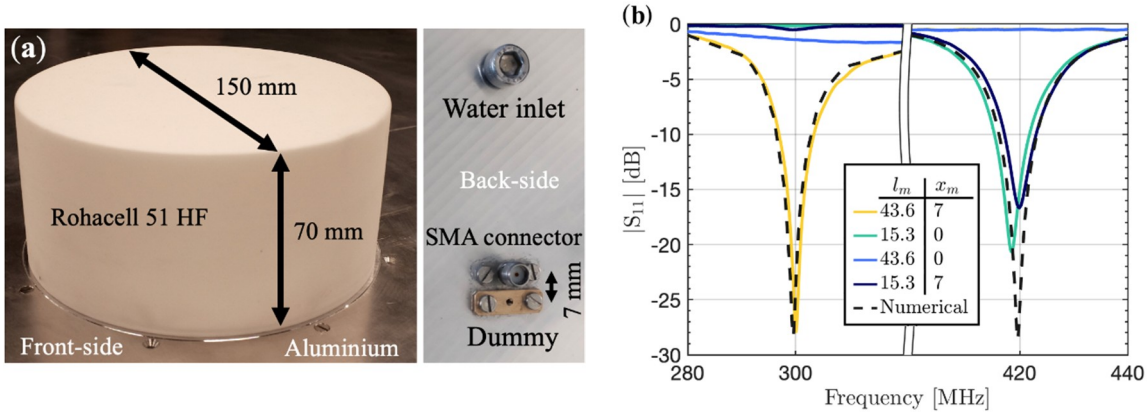

Figure 3. (**a**) Photographs of the front and back of the fabricated antenna and (**b**) measured reflection coefficient with different displacement positions x_m and monopole antenna lengths l_m, both in mm. Water temperature was 19–20 °C. The numerical results are shown with the optimized antenna lengths and positions at 20 °C.

In Figure 4a, the electric field distribution in the xz-plane of the magnetic dipole antenna is shown at 300 MHz. From the direction of the electric field (shown by the arrows), it is clear why the monopole cannot be positioned in the center of the hemisphere ($x_m \neq 0$) if the magnetic resonance is to be excited. In order to excite a circulating electric displacement current, the monopole has to be displaced from the center of the hemisphere.

The calculated radiation pattern for the magnetic dipole antenna is shown in Figure 4b by the normalized radiation intensity in the xz- and xy-planes. It can be seen that there was no radiation in the negative z direction because of the ground plane. The radiation pattern was similar to that of a half-loop antenna, while the radiation pattern of the electric dipole antenna was similar to that of the monopole antenna (see Appendix B.2). The magnetic (electric) dipole antenna had isotropic radiation in the xz-plane (xy-plane) with the maximum realized gain (G_{real}) of 0.16 dBi (–3.1 dBi).

The radiation pattern was also measured with a simple dipole antenna designed for 300 MHz. By rotating the antenna under test, the transmission coefficient was measured at different angles in the xz-plane of the antenna. The normalized transmission coefficient is included in Figure 4b. From 0° to ±90°, the measurements were similar to the numerical results. However, at higher angles, they started to deviate. This was expected because the simulated ground plane was infinite, whereas a ground plane of 1 m diameter was used in the measurements.

The 3 dB fractional bandwidth, FBW_{3dB}, of the magnetic (electric) dipole antenna was 7.81% (2.85%). This gave a radiation quality factor, Q, of 1.06 (22.4) times the so-called lower bound, Q_{lb}, (also known as the Chu limit, see Appendix A) with $k_0a \approx 0.35$ ($k_0a \approx 0.46$) for the magnetic (electric) dipole antenna. As $k_0a \leq 0.5$ for both antennas, they are electrically small. For a quarter wavelength monopole, $k_0a = \pi/2$; thus, water reduced the size of the antenna by a factor of 4.5 (3.2). Moreover, the magnetic dipole water-based DRA reported herein represents the electrically smallest water-based antenna to date. The cost is a reduction in radiated power (and thus the total efficiency) due to the losses in water as well as the bandwidth. Nevertheless, its fractional bandwidth is higher than many other compact antennas [9,10]. In addition, bearing in mind that the present design does not require any expensive or rare materials, the antenna will be very cheap and easy to produce. Furthermore, water adds flexibility to the design, allowing tuning by temperature and extraction of water, which we have examined both numerically and experimentally. The results are included in Appendix B.3.

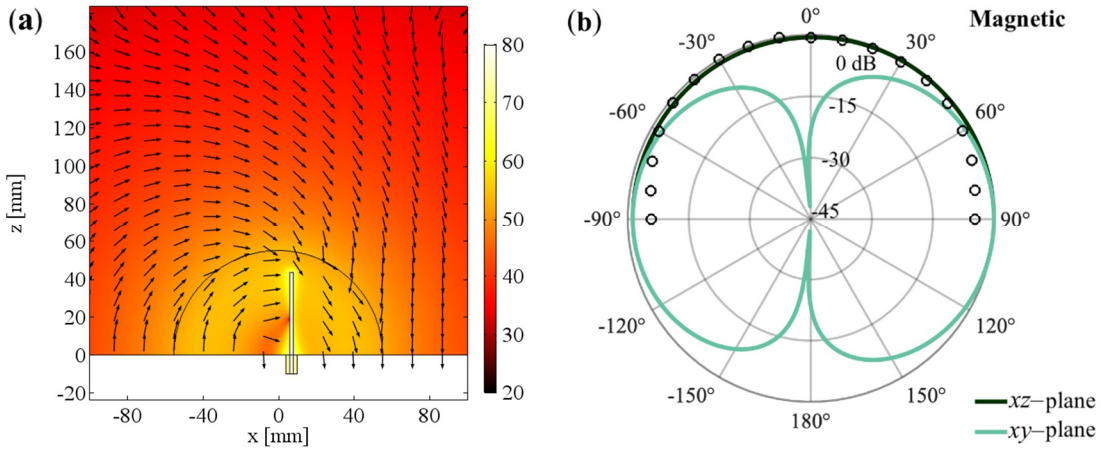

Figure 4. (**a**) The electric field distribution in the *xz*-plane for the magnetic dipole antenna. The colors show the intensity of the electric field in logarithmic scale, whereas the arrows show the direction. (**b**) Radiation pattern shown by the normalized radiation intensity in the *xz* - and *xy*-planes for the magnetic dipole antenna. The black circles show the measured radiation pattern. See Appendix B.2 for the electric field intensity and radiation pattern for the electric dipole antenna.

4. Conclusions

In summary, simple electrically small water-based DRAs were investigated both numerically and experimentally. The fundamental resonances were excited in a water hemispherical cavity and used to effectively match a short monopole antenna to both its feed line and the surrounding free space. The final antennas were optimized by varying the length and the displacement of the monopole. As a result, compact water-based DRAs were designed. The optimum antenna had an electrical size of $\lambda_0/18$, making it the smallest water-based antenna to date, albeit with lowered total efficiency due to water losses. We believe that the proposed electrically small water-based DRAs may serve as cheap and easy-to-fabricate tunable alternatives for VHF and the low end of UHF bands.

Author Contributions: Formal analysis, software, investigation, and writing—original draft preparation, R.E.J.; supervision and writing—review and editing, A.V.L. and S.A.

Funding: This research received no external funding.

Acknowledgments: The authors would like to thank the workshop at the Electromagnetic Systems group of the Technical University of Denmark for fabrication of the antennas.

Conflicts of Interest: The authors declare no conflict of interest.

Appendix A

This appendix presents the definition of the antenna parameters used in this work. The water-based DRA can be described by the equivalent circuit diagram in Figure A1. We were interested in maximizing the total efficiency given by [2]:

$$\eta_{\text{eff}} = \frac{P_{\text{rad}}}{P_{\text{in}}} = \eta_{\text{rad}}\left(1 - |S_{11}|^2\right) \tag{A1}$$

where P_{rad} is the total radiated power, and P_{in} is the input power to the transmission line. $\eta_{\text{rad}} = P_{\text{rad}}/(P_{\text{rad}} + P_{\text{d}})$ is the radiation efficiency, with P_{d} being the power dissipated in the antenna, and $|S_{11}|^2 = P_{\text{r}}/P_{\text{in}}$ is the fraction of the power reflected (P_{r}) due to mismatch of the antenna input impedance (Z_{A}) to that of the transmission line (Z_0). S_{11} designates the antenna reflection coefficient.

We characterized the impedance bandwidth of the antenna by the 3 dB fractional voltage standing wave ratio (VSWR) bandwidth $\text{FBW}_{3\text{dB}} = (f_{-3\text{dB}} - f_{+3\text{dB}})/f_0$, with $f_{\pm 3\text{dB}}$ being the ±3 dB frequencies

of S_{11} and f_0 being the resonance frequency [3]. For electrically small antennas, the quality factor $Q = 2/\mathrm{FBW}_{3\mathrm{dB}}$, and presently we applied the following ratio:

$$Q_{\mathrm{ratio}} = \frac{Q}{Q_{\mathrm{lb}}} \tag{A2}$$

with $Q_{\mathrm{lb}} = b_i \eta_{\mathrm{rad}} Q_{\mathrm{Chu}} = b_i \eta_{\mathrm{rad}} \left(\frac{1}{k_0 a} + \frac{1}{(k_0 a)^3} \right)$ being the lower bound of Q, where b_i is a resonance mode factor with $i = \mathrm{m}, \mathrm{e}$ denoting the mode, and Q_{Chu} is the Chu limit [1–5]. For magnetic (electric) resonant antennas, $b_{\mathrm{m}} = 3$ ($b_{\mathrm{e}} = 1.5$). We used Equation (A2) to determine how close the Q of the antenna was to the theoretical minimum.

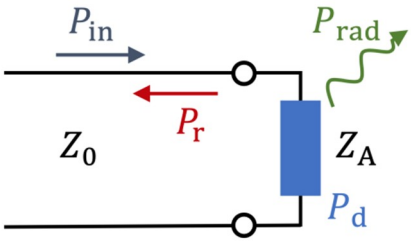

Figure A1. Equivalent circuit diagram of antenna.

The realized antenna gain in a given direction can be calculated as follows [2]:

$$G_{\mathrm{real}}(\theta, \phi) = \eta_{\mathrm{eff}} D(\theta, \phi) \tag{A3}$$

where $D(\theta, \phi) = 4\pi U(\theta, \phi)/P_{\mathrm{rad}}$ is the directivity, with $U(\theta, \phi)$ being the radiation intensity and (θ, ϕ) denoting the direction of radiation.

Appendix B

This appendix contains the additional results for the scattering analysis of a water sphere and the electric dipole antenna as well as the sensitivity and tunability of the antennas.

Appendix B.1 Scattering Analysis of Water Sphere

The solution to a plane wave incidence on a dielectric sphere is well known [29], and it was studied in a previous work [30]. The configuration is shown in Figure A2a. The amplitude coefficients are [29]

$$a_n = \frac{\varepsilon_{\mathrm{r,w}} j_n(k_{\mathrm{w}} r_{\mathrm{w}}) j_n{}'(k_0 r_{\mathrm{w}}) - j_n{}'(k_{\mathrm{w}} r_{\mathrm{w}}) j_n(k_0 r_{\mathrm{w}})}{\varepsilon_{\mathrm{r,w}} j_n(k_{\mathrm{w}} r_{\mathrm{w}}) h_n^{(2)}{}'(k_0 r_w) - j_n{}'(k_{\mathrm{w}} r_{\mathrm{w}}) h_n^{(2)}(k_0 r_{\mathrm{w}})} \tag{A4}$$

$$b_n = \frac{j_n(k_w r_{\mathrm{w}}) j_n{}'(k_0 r_{\mathrm{w}}) - j_n{}'(k_{\mathrm{w}} r_{\mathrm{w}}) j_n(k_0 r_{\mathrm{w}})}{j_n(k_{\mathrm{w}} r_{\mathrm{w}}) h_n^{(2)}{}'(k_0 r_{\mathrm{w}}) - j_n{}'(k_{\mathrm{w}} r_{\mathrm{w}}) h_n^{(2)}(k_0 r_{\mathrm{w}})} \tag{A5}$$

for the TM^r and TE^r scattering field components, respectively. $\varepsilon_{\mathrm{r,w}}$ and k_w are the relative permittivity and the wavenumber in water, respectively. j_n and $h_n^{(2)}$ are the nth order spherical Bessel function of the first kind and spherical Hankel function of the second kind, respectively. The prime $'$ denotes the operation $g_n{}'(x) = d[x g_n(x)]/dx$.

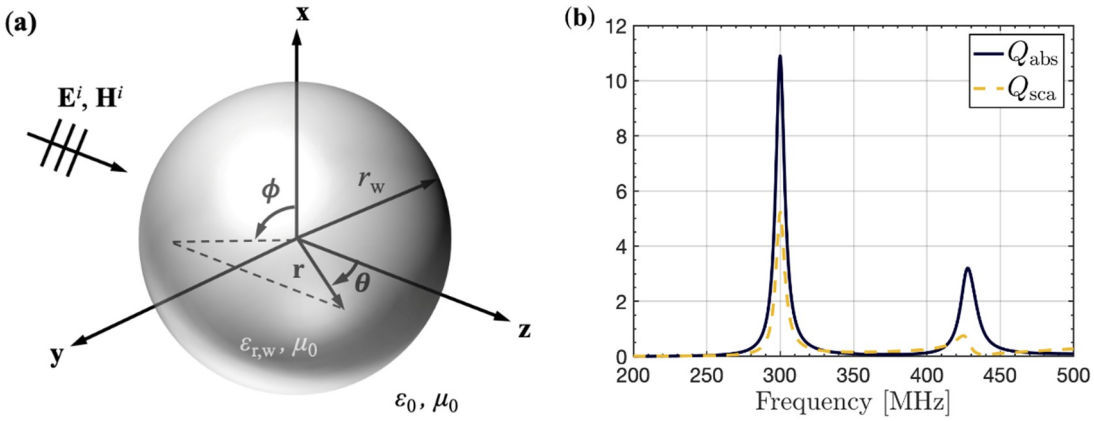

Figure A2. (**a**) Sketch of the water sphere in free space illuminated by a plane wave and (**b**) the spectrum of the scattering and absorption efficiencies for a sphere with $r_w = 55.18$ mm and a water temperature of 20 °C.

The absorption, extinction, and scattering efficiencies were used to describe the response of the water sphere, and they are related by $Q_{abs} = Q_{ext} - Q_{sca}$, where

$$Q_{sca} = \frac{2}{(k_0 r_w)^2} \sum_{n=1}^{\infty} (2n+1)\left(|a_n|^2 + |b_n|^2\right) \tag{A6}$$

$$Q_{ext} = \frac{2}{(k_0 r_w)^2} \sum_{n=1}^{\infty} (2n+1)\mathrm{Re}\{a_n + b_n\}. \tag{A7}$$

The spectrum of the scattering and absorption efficiencies are shown in Figure A2b for a sphere with $r_w = 55.18$ mm and a water temperature of 20 °C. Peaks at 300 and 430 MHz can be seen, caused by the magnetic dipole (b_1) and electric dipole (a_1) resonances, respectively. These were the resonances that we utilized in the antennas. We found that 32% (68%) of the extinct power was scattered (absorbed) at the magnetic dipole resonance frequency, which was very similar to the efficiency found for the magnetic dipole antenna.

Appendix B.2 Electric Dipole Antenna for 300 MHz

The electric field distribution in the *xz*-plane at 300 MHz is shown in Figure A3a. The calculated radiation pattern is shown in Figure A3b by the normalized radiation intensity in the *xz*- and *xy*-planes. The field distribution was symmetrical as the monopole was positioned in the center of the hemisphere. Notice that there was no radiation in the negative *z* direction because of the ground plane.

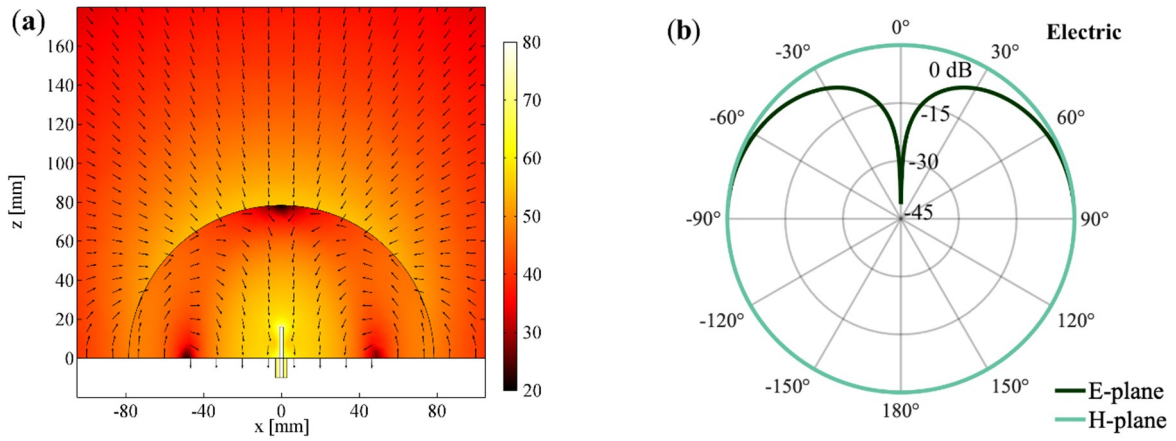

Figure A3. (**a**) The electric field distribution in the *xz*-plane as well as (**b**) the radiation pattern in the *xz* - and *xy*-plane for electric dipole antenna. The colors in (**a**) show the intensity of the electric field in logarithmic scale, whereas the arrows show the direction.

Appendix B.3 Sensitivity and Tunability

Variation in the cable type of same characteristic impedance had a minimum impact on the radiated power. The same was the case for the length of the transmission line below the ground plane (l_c). However, variation of the length and position of the monopole (Δl_m and Δx_m) as well as the hemisphere radius and temperature of water (Δr_w and ΔT_w) affected the radiated power. Analysis of the different parameters showed that changes of $\Delta l_m \approx 1.7$ mm, $\Delta x_m \approx 0.7$ mm, $\Delta V_w \approx 1.4$ mL, and $\Delta T_w \approx 0.4$ °C resulted in a 1% decrease in radiated power for the magnetic dipole antenna at 300 MHz. This information is important because it shows how sensitive the antenna is to fabrication imperfections. However, this can also be seen as a way to tune the antenna. This is illustrated in Figure A4 by the results of simulated temperature tuning and measurements of water extraction from the hemisphere for the magnetic dipole antenna. In Figure A4a, the total efficiency as a function of frequency and temperature is shown. Clearly, the resonance frequency was shifted by a change in temperature. From 0 to 100 °C, the peak of the efficiency was blue-shifted linearly (as indicated by the black tendency line) from 286 to 358 MHz, corresponding to a shift of 25%. This blue-shift was obviously due to the permittivity of water changing from $87.8 - j2.8$ to $55.8 - j0.22$, effectively bringing a change of 25% to the wavenumber in water. Furthermore, the temperature growth decreased the losses in water, and the total efficiency was above 50% from around 55 °C.

The reflection coefficient was moreover measured for different water fillings extracting 1% (≈3.5 mL) volume of water at the time from the completely filled hemisphere. During the measurements, the ground plane was kept in horizontal level. The results are shown in Figure A4b, and it can be seen that there was a linear blue-shift and increment of the minimum in the reflection coefficient as water was extracted, demonstrating yet another means of tunability in the water-based antenna.

The tunability properties of the antenna can, in principle, also be used for sensing. Several antennas designed for sensing temperature changes of up to 1000 °C have already been demonstrated [31–33].

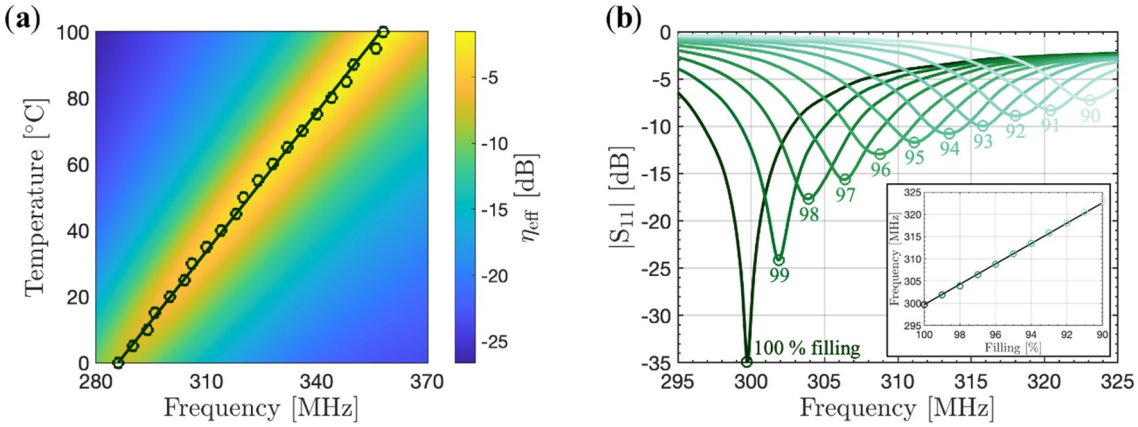

Figure A4. (**a**) Simulated temperature tuning and (**b**) experimental water fill tuning for the magnetic dipole antenna. The black circles and line in (**a**) indicate the maximum efficiency at each 5 °C temperature and the tendency, respectively. The inset in (**b**) shows the frequency of the minimum reflection coefficient for each filling.

References

1. Chu, L.J. Physical limitations of omnidirectional antennas. *J. Appl. Phys.* **1948**, *19*, 1163–1175. [CrossRef]
2. Balanis, C.A. *Antenna Theory*, 3rd ed.; Wiley: New York, NY, USA, 2005; Volume 64–69, pp. 637–641.
3. Yaghjian, A.D.; Best, S.R. Impedance, bandwidth, and Q of antennas. *IEEE Trans. Antennas Propag.* **2005**, *53*, 1298–1324. [CrossRef]
4. Thal, H.L. New radiation Q limits for spherical wire antennas. *IEEE Trans. Antennas Propag.* **2006**, *44*, 2757–2763. [CrossRef]
5. Best, S.R. The radiation properties of electrically small folded spherical helix antennas. *IEEE Trans. Antennas Propag.* **2004**, *52*, 953–960. [CrossRef]
6. Best, S.R. Low Q electrically small linear and elliptically polarized spherical dipole antennas. *IEEE Trans. Antennas Propag.* **2005**, *53*, 1047–1053. [CrossRef]
7. Erentok, A.; Kim, O.S.; Arslanagić, S. Cylindrical metamaterial-based subwavelength antenna. *Microw. Opt. Technol. Lett.* **2009**, *51*, 1496–1500. [CrossRef]
8. Ziolkowski, R.W.; Erentok, A. Metamaterial-based efficient electrically small antennas. *IEEE Trans. Antennas Propag.* **2006**, *54*, 2113–2130. [CrossRef]
9. Erentok, A.; Ziolkowski, R.W. Metamaterial-inspired efficient electrically small antennas. *IEEE Trans. Antennas Propag.* **2008**, *56*, 691–707. [CrossRef]
10. Petosa, A.; Ittipiboon, A. Dielectric Resonator Antennas: A Historical Review and the Current State of the Art. *IEEE Antenn. Propag. Mag.* **2010**, *52*, 91–116. [CrossRef]
11. Kingsley, S.P.; O'Keefe, S.G. Beam steering and monopulse processing of probe-fed dielectric resonator antennas. *Proc. IEEE Radar Sonar Navig.* **1999**, *146*, 121–125. [CrossRef]
12. Ellison, W. Permittivity of pure water, at standard atmospheric pressure, over the frequency range 0–25 THz and the temperature range 0–100 °C. *J. Phys. Chem. Ref. Data* **2007**, *36*, 1–18. [CrossRef]
13. O'Keefe, S.G.; Kingsley, S.P. Tunability of liquid dielectric resonator antennas. *IEEE Antennas Wirel. Propag. Lett.* **2007**, *6*, 533–536. [CrossRef]
14. Zhou, R.; Zhang, H.; Xin, H. Liquid-based dielectric resonator antenna and its application for measuring liquid real permittivities. *IET Microw. Antennas Propag.* **2014**, *8*, 255–262. [CrossRef]
15. Mobashsher, A.T.; Abbosh, A. Reconfigurable water-substrate based antennas with temperature control. *Appl. Phys. Lett.* **2017**, *110*, 253503. [CrossRef]
16. Li, Y.; Luk, K.M. A water dense dielectric patch antenna. *IEEE Access* **2015**, *3*, 274–280. [CrossRef]
17. Sun, J.; Luk, K.M. A wideband low cost and optically transparent water patch antenna with omnidirectional conical beam radiation patterns. *IEEE Trans. Antennas Propag.* **2017**, *65*, 4478–4485. [CrossRef]

18. Chen, Y.; Wang, C. Dual-band directional/omni-directional liquid dielectric resonator antenna designs using characteristic modes. In Proceedings of the IEEE Antennas and Propagation Society International Symposium (APSURSI), Memphis, TN, USA, 6–11 July 2014; pp. 848–849.
19. Xing, L.; Huang, Y.; Xu, Q.; Aljaafreh, S. Wideband, hybrid rectangular water antenna for DVB-H applications. *Microw. Opt. Technol. Lett.* **2015**, *59*, 2160–2164. [CrossRef]
20. Fayad, H.; Record, P. Broadband liquid antenna. *Electron. Lett.* **2006**, *42*, 133–134. [CrossRef]
21. Xing, L.; Huang, Y.; Shen, Y.; Al Ja'afreh, S.; Xu, Q.; Alrawashdeh, R. Further investigation on water antennas. *IET Microw. Antennas Propag.* **2015**, *9*, 735–741. [CrossRef]
22. Xing, L.; Meng, X.; Yang, L.; Xu, B.; Pan, Y. A wideband water antenna for WiFi applications. In Proceedings of the International Workshop on Antenna Technology (iWAT), Nanjing, China, 5–7 March 2018; pp. 1–3.
23. Andryieuski, A.; Kuznetsova, S.M.; Zhukovsky, S.V.; Kivshar, Y.S.; Lavrinenko, A.V. Water: Promising opportunities for tunable all—Dielectric electromagnetic metamaterials. *Sci. Rep.* **2015**, *5*, 13535. [CrossRef]
24. Gorlach, M.A.; Song, M.; Slobozhanyuk, A.P.; Bogdanov, A.A.; Belov, P. Topological transition in coated wire medium. *Phys. Status Solidi RRL* **2016**, *10*, 900–904. [CrossRef]
25. Yang, X.; Zhang, D.; Wu, S.; Li, L.; Cao, K.; Huang, K. Reconfigurable all-dielectric metasurface based on tunable chemical systems in aqueous solution. *Sci. Rep.* **2017**, *7*, 3190. [CrossRef]
26. Jacobsen, R.E.; Lavrinenko, A.V.; Arslanagić, S. Water-Based Metasurfaces for Effective Switching of Microwaves. *IEEE Antennas Wirel. Propag. Lett.* **2018**, *17*, 571–574. [CrossRef]
27. Yoo, Y.J.; Ju, S.; Park, S.Y.; Kim, Y.J.; Bong, J.; Lim, T.; Kim, K.W.; Rhee, J.Y.; Lee, Y.P. Metamaterial absorber for electromagnetic waves in periodic water droplets. *Sci. Rep.* **2015**, *5*, 14018. [CrossRef]
28. COMSOL Multiphysics 5.3. Available online: https://www.comsol.com/ (accessed on 4 October 2019).
29. Bohren, C.F.; Huffman, D.R. *Absorption and Scattering of Light by Small Particles*, 1st ed.; Wiley: Weinheim, Germany, 1998; pp. 82–129.
30. Jacobsen, R.E.; Arslanagić, S.; Lavrinenko, A.V. Fundamental properties of Mie resonances in water spheres. In Proceedings of the URSI International Symposium on Electromagnetic Theory (EMTS), San Diego, CA, USA, 27–31 May 2019.
31. Boccard, J.-M.; Aftab, T.; Hoppe, J.; Yousaf, A.; Hütter, R.; Reindl, L.M. High-resolution, far-field, and passive temperature sensing up to 700 °C using an isolated ZST microwave dielectric resonator. *IEEE Sens. J.* **2016**, *16*, 715–722. [CrossRef]
32. Cheng, H.; Ebadi, S.; Gong, X. A low-profile wireless passive temperature sensor using resonator/antenna integration up to 1000 °C. *IEEE Antennas Wirel. Propag. Lett.* **2012**, *11*, 369–372.
33. Yao, J.; Tchafa, F.M.; Jain, A.; Tjuatja, S.; Huang, H. Far-field interrogation of microstrip patch antenna for temperature sensing without electronics. *IEEE Sens. J.* **2016**, *16*, 7053–7060. [CrossRef]